ACS APPLIED ELECTRONIC MATERIALS

pubs.acs.org/acsaelm Article

All-Oxide NiO/Ga_2O_3 p−n Junction for Self-Powered UV Photodetector

Yachao Wang, Chao Wu, Daoyou Guo,* Peigang Li, Shunli Wang, Aiping Liu,* Chaorong Li,* Fengmin Wu, and Weihua Tang

Cite This: *ACS Appl. Electron. Mater.* 2020, 2, 2032−2038

Read Online

ACCESS | Metrics & More | Article Recommendations

ABSTRACT: Recently, Ga_2O_3-based self-powered ultraviolet photodetectors have aroused great interest due to their potential applications in civil, medical, and environmental monitoring fields. So far, most p−n junction photodetectors are fabricated with p-type semiconductors like GaN and SiC, which are usually nonoxide materials. As a result, the p-type semiconductors are oxidized and the conductive properties degenerated when constructing a p−n junction with the Ga_2O_3 thin film at a high growth temperature. In this work, we chose the oxide NiO as the p-type material and used radio-frequency reactive magnetron sputtering system to fabricate the all-oxide NiO/Ga_2O_3 p−n junction at room temperature and manufacture the self-powered UV photodetector. Thanks to the type II band alignment, the photodetector exhibits a responsivity (R) of 57 μA/W, a detectivity (D^*) of 5.45×10^9 jones, and an I_{light}/I_{dark} ratio of 122 when exposed to a 254 nm light irradiation at 0 V. In addition, the photodetector based on the all-oxide NiO/Ga_2O_3 p−n junction shows good stability and reproducibility in air, oxygen, and vacuum. Our results provide an inexpensive and suitable pathway for the mass production of self-powered UV photodetectors.

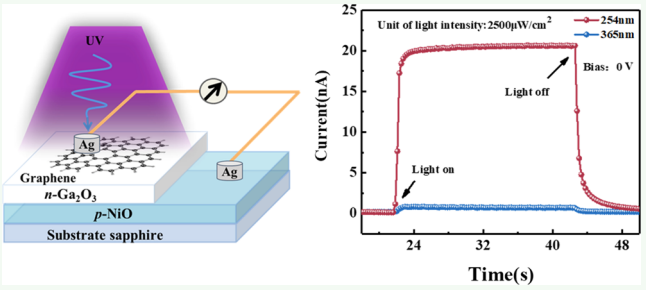

KEYWORDS: *self-powered, all-oxide, ultraviolet photodetector, NiO, Ga_2O_3, p−n junction*

INTRODUCTION

Recently, ultraviolet (UV) photodetectors have aroused the widespread concern of researchers around the world for their wide applications in UV radiation detection, missile warning, flame detection, ozone monitoring, and environmental monitoring.[1−5] In general, traditional UV photodetectors always need external power. However, they are not suitable for energy-saving and environment nowadays, especially the materials for batteries are unfriendly for human health. These photodetectors based on p−n junction, heterojunction, or Schottky barrier can work without an external voltage. Thanks to the built-in electric field, the electron−hole pairs can separate automatically,[6−8] which not only has the benefit of energy-saving but also makes it possible to work in Antarctic/Arctic and outer space for a long time.

Gallium oxide (Ga_2O_3) is a promising wide band gap semiconductor that exhibits many natural advantages over other materials, especially in developing self-powered UV photodetectors.[9−13] In recent years, many reports have been published in this area, which has attracted widespread attention. Because of the intrinsic oxygen deficiency, hydrogen doping, Si impurities, etc., Ga_2O_3 behaves as an n-type oxide semiconductor.[14−18] Therefore, it can form a p−n junction for self-powered UV photodetectors with some p-type semiconductor materials, including GaN,[19−21] SiC,[22−24] etc.[25,26] These photodetectors exhibit satisfactory photoresponsivity under the bias of 0 V. For example, our group[20,21] constructed self-powered UV photodetectors using GaN/Ga_2O_3 and GaN/Sn:Ga_2O_3 p−n junction with the responsivity of 28.44 mA/W and 3.05 A/W. Shen et al.[27] manufactured a self-powered Au/β-Ga_2O_3 nanowire array film Schottky junction with a responsivity of 0.01 mA/W. Jia et al.[24] prepared a β-Ga_2O_3/4H−SiC p−n junction device with a responsivity of 10.35 mA/W. Among these self-powered structures, photodetectors based on p−n junction are more attractive, while Schottky-type photodetectors have limitations such as small open circuit (V_{oc}), light reflection by metals, and insufficient depletion width. However, the p-type semiconductor used in the Ga_2O_3-based p−n junction self-powered UV photodetectors usually are nonoxide materials, like the above-mentioned GaN and SiC. Thus, the p-type semiconductor is oxidized when the

Received: April 13, 2020
Accepted: June 10, 2020
Published: June 10, 2020

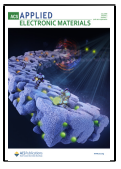

https://dx.doi.org/10.1021/acsaelm.0c00301
ACS Appl. Electron. Mater. 2020, 2, 2032−2038

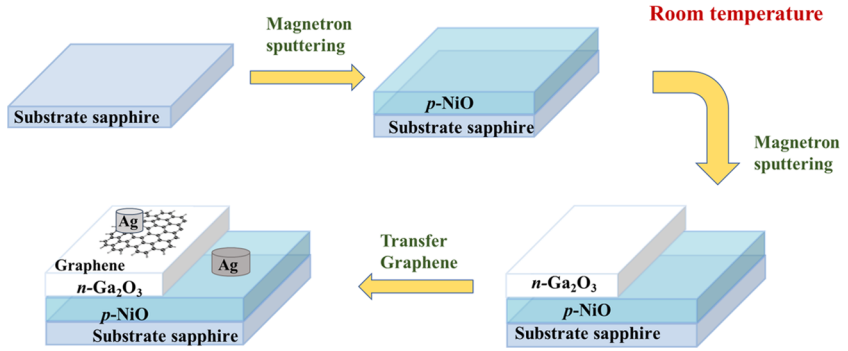

Figure 1. Illustration of the preparation process of the NiO/Ga_2O_3 p−n junction.

crystallized Ga_2O_3 thin film is grown on it under a high growth temperature and its conductive properties are affected. As a result, the built-in electric field, which originates from the p−n junction, is diluted. Therefore, it is necessary to find a p-type oxide semiconductor material that would constitute a high-performance p−n junction self-powered photodetector.

NiO as a natural p-type oxide semiconductor has attracted a lot of attention owing to its 3.2−3.8 eV band gap with excellent chemical stability, nontoxicity, and high visible-light transmittance.[28−33] In addition, the large excitonic binding energy (110 meV) makes it more widely used than other semiconductors such as GaN and ZnO.[34] Recently, some research studies have demonstrated that there is a good matching epitaxial relation and band structure between NiO and Ga_2O_3.[35−37] For example, NiO/β-Ga_2O_3 heterojunction diodes have been built by the sol−gel method and exhibit a rectifying ratio greater than 10^8 at a bias of ±3 V. Also, the UV photodetectors based on NiO and Ga_2O_3 have attracted the attention of the researchers. Li et al.[38] prepared a β-Ga_2O_3/NiO heterojunction diode that exhibits a responsivity of 415 mA/W under 7 V but did not investigate the self-powered photoelectric properties.

In our work, we use a radio-frequency (RF) reactive magnetron sputtering system to fabricate an all-oxide NiO/Ga_2O_3 p−n junction at room temperature. To construct the photodetector, monolayer graphene is used as the top electrode. Graphene is a transparent conductive film composed of a layer of carbon; due to good electrical conductivity and UV/extreme UV optical transparency, it can be used to increase the transmittance of the incident light and improve the photoresponsivity.[39−41] Thanks to the novel construction, the photodetector exhibits a photoresponse time of 0.34 s and an I_{light}/I_{dark} ratio of 122 to a 254 nm light illumination at zero bias. Due to the existence of surface defects, the conductivity and photoresponse of the NiO/Ga_2O_3 p−n junction are affected by the absorption and desorption of O_2 molecules. Under the 254 nm light illumination, a maximum photoresponsivity of 147 μA/W and the slowest photoresponse time of 0.69/3.95 s (τ_r/τ_d) were obtained under oxygen and the fastest photoresponse time of 0.20/2.51 s (τ_r/τ_d) was obtained under a vacuum.

RESULTS AND DISCUSSION

The schematic diagram of the preparation process of the all-oxide NiO/Ga_2O_3 p−n junction photodetector is illustrated in Figure 1 (see the Experimental Section for details). Figure 2a shows the XRD patterns of a NiO thick film (4 μm), a Ga_2O_3 thin film (200 nm), and a NiO (4 μm)/Ga_2O_3 (200 nm) p−n junction grown on the (0001) Al_2O_3 substrates. The wider (111) oriented diffraction peak of NiO at 36.5° is found in the NiO thick film, indicating microcrystallinity. As for the Ga_2O_3 thin films grown on Al_2O_3 substrates, there is no obvious peak except an indistinct diffraction peak at about 25°, which can be interpreted as the stacking of the amorphous grain. For the NiO/Ga_2O_3 p−n junction, the intensity of the diffraction peak corresponding to the (111) reflection is weaker than that of the NiO film directly grown on the Al_2O_3 substrate, which can be explained by the existence of the Ga_2O_3 films on the top layer. In Figure 2b, the NiO film shows an absorption edge at wavelengths of about 350 nm, which is consistent with the band gap of ∼3.60 eV (the inset of Figure 2b). Since the material is amorphous, we used Tauc plots of $(\alpha h\nu)^{1/2}$ to estimate the band gap.[42,43] Here, the absorption follows a power law of the form provided by Tauc

$$(\alpha h\nu)^{1/2} = A(h\nu - E_g)$$

Similarly, the Ga_2O_3 film shows an absorption edge at wavelengths of about 255 nm (Figure 2c), which corresponds to the band gap of ∼4.80 eV (the inset of Figure 2c). Figure 2d shows the cross-sectional image of the NiO/Ga_2O_3 p−n junction. The thicknesses of the Ga_2O_3 and NiO layers are estimated to be about 200 nm and 4 μm, respectively.

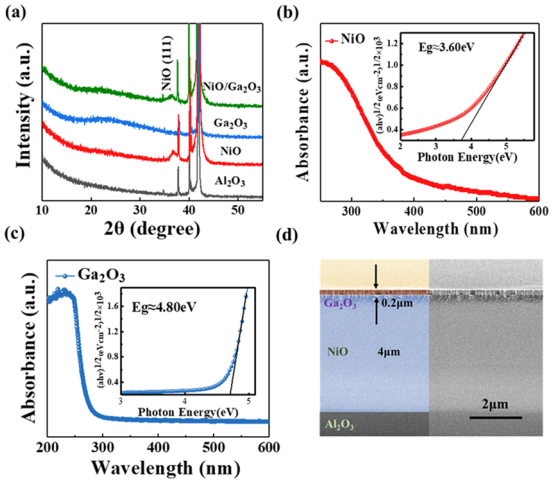

Figure 2. (a) XRD patterns of a 4 μm thick NiO film, 200 nm thick Ga_2O_3 film, and a NiO (4 μm)/Ga_2O_3 (200 nm) p−n junction grown on the (0001) Al_2O_3 substrate. Absorption spectra for (b) NiO films and (c) Ga_2O_3 films. (d) Cross-sectional scanning electron microscopy (SEM) image of the NiO/Ga_2O_3 p−n junction deposited on the Al_2O_3 substrate.

https://dx.doi.org/10.1021/acsaelm.0c00301
ACS Appl. Electron. Mater. 2020, 2, 2032−2038

Figure 3c displays the schematic diagram of the NiO/Ga_2O_3 p−n junction photodetector. Before studying the $I-V$

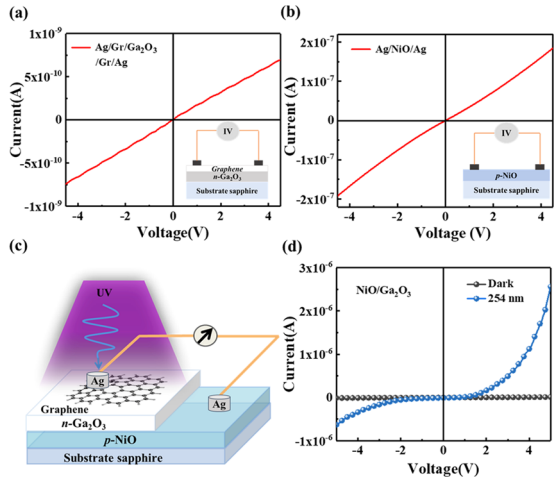

Figure 3. $I-V$ plots of (a) Ag/graphene/Ga_2O_3/graphene/Ag structure and (b) Ag/NiO/Ag structure. (c) Schematic illustration of the fabricated prototype NiO/Ga_2O_3 p−n junction. (d) $I-V$ plots of the device based on the NiO/Ga_2O_3 p−n junction under dark and 254 nm light illumination.

characteristics of the NiO/Ga_2O_3 p−n junction, we investigate the contacts of the Ag/graphene/Ga_2O_3/graphene/Ag and Ag/NiO/Ag interface, which can be seen in Figure 3a,b. The $I-V$ curves exhibit a linear characteristic, indicating that Ag and graphene electrodes form ohmic contact with the Ga_2O_3 and NiO films. The linear $I-V$ curve of the detector consisting of the NiO/Ga_2O_3 p−n junction under dark and a 254 nm light is shown in Figure 3d. The inset shows logarithmic $I-V$ features. An on/off ratio (I_{254nm}/I_{dark}) of 208 can be obtained at a 5 V bias. The asymmetric ratio, I_{254nm} (5 V)/I_{254nm} (−5 V) = 2.56/−0.62 μA, is ∼4.13. The result reflects a typical rectifying characteristic, indicating the successful formation of the p−n junction.

To further illustrate the time-dependent photoresponse of the detector under illumination, the 254 and 365 nm UV lights are switched on and off periodically under a zero-bias voltage, while the light intensity of each UV radiation is 2500 $\mu W/cm^2$. As shown in Figure 4a, the dark current is about 0.17 nA. When the detector is irradiated with the 254 nm light, the current increases to 20.73 nA rapidly. The ratio I_{photo}/I_{dark} is approximately 122. When the 365 nm UV light is switched on, the photoresponse of the detector is not obvious and the photocurrent is approximately 0.82 nA. These results indicate that light absorption is mainly concentrated in the Ga_2O_3 layer. Figure 4b shows the relationship between the photocurrent and the light intensity, while the intensity ranges from 100 to 2500 $\mu W\ cm^2$ at a zero-bias voltage. The regular step type curve shows the stability and the fast response of the photocurrent. As shown in Figure 4c, the photocurrent increases from 3.25 to 20.73 nA with a nonlinear increasing trend with the gradual increase in light intensity. The photocurrent (I_{ph}) as a function of the incident light intensity (P) can be explained by the law $I_{ph} \propto P^{\gamma}$, where γ is the exponent. Obviously, the experimental γ value is less than 1, which can be attributed to the intrinsic defects, charge impurities, and carrier recombination between the NiO/Ga_2O_3 p−n junction. Responsivity (R) is a key parameter to

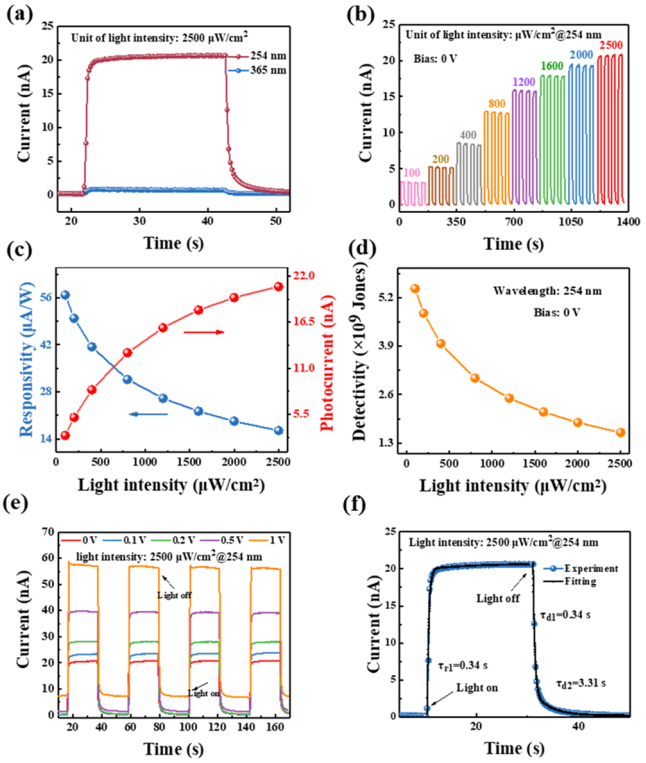

Figure 4. (a) Continuous time-dependent photoresponse of the NiO/Ga_2O_3 p−n junction under a zero bias at 254 and 365 nm illumination with a light intensity of 2500 $\mu W/cm^2$. (b) Time-dependent photoresponse of the photodetector under a zero bias and a 254 nm light with various light intensities. (c) Photocurrent and responsivity as a function of light intensity. (d) Detectivity as a function of light intensity. (e) Time-dependent photoresponse of the photodetector under various biases with a 254 nm light illumination. (f) Enlarged view of the rise/decay edges and the corresponding exponential fitting.

assess the performance of the detector, and it can be expressed as

$$R = \frac{I_{photo} - I_{dark}}{P^*S}$$

where S is the effective area of the detector (∼0.5 cm^2). The increase in the incident light intensity (100−2500 $\mu W\ cm^2$) not only generates more electron−hole pairs but also induces self-heating. Subsequently, the probability of a charge-carrier scattering and recombination is also increased, resulting in a decrease in responsivity (57−16 $\mu A/W$). Detectivity (D^*) is a pivotal parameter to evaluate the capability of a photodetector to describe the smallest detectable signals, which can be expressed as

$$D^* = \frac{R_\lambda}{\sqrt{2qJ_d}}$$

By calculation, the maximum D^* of 5.45×10^9 jones is attained at 100 $\mu W\ cm^2$ light illumination (Figure 4d). Figure 4e shows the effect of the bias voltage on the photoresponse of the detector. At a higher bias, more carriers are released from the oxygen vacancy traps and the dark current is increased. At the same time, the photogenerated electron−hole pairs are separated effectively, resulting in an increase in photocurrent. The fitting curve of the photoresponse is shown in Figure 4f,

https://dx.doi.org/10.1021/acsaelm.0c00301
ACS Appl. Electron. Mater. 2020, 2, 2032−2038

and it can be fitted by a formula with two relaxation-time constants (τ_1 and τ_2) as follows

$$I = I_0 + Ae^{-t/\tau_1} + Be^{-t/\tau_2}$$

where I_0 is the dark photocurrent, t is the time, A and B are constants, the constant τ_1 is related to the rapid change in the carrier concentration when the UV light is turned on/off, and τ_2 is related to carrier trapping and release due to the oxygen vacancy defects in the amorphous films. The curves can be well fitted, with the response time (τ_r) of 0.34 s and the decay time (τ_d) of 3.65 s.

To comprehend the microscopic mechanism of the self-powered characteristic of the NiO/Ga_2O_3 p−n junction, the energy band structure is explained by X-ray photoelectron spectroscopy (XPS) measurement. According to the relation presented by Kraut,[44] the valence band offset (VBO) at the NiO/Ga_2O_3 p−n junction can be calculated by

$$\Delta E_V = (E^{NiO}_{Ni\ 2p_{3/2}} - E^{NiO}_{VBM}) - (E^{Ga_2O_3}_{Ga\ 2p_{3/2}} - E^{Ga_2O_3}_{VBM}) + (E^{NiO/Ga_2O_3}_{Ga\ 2p_{3/2}} - E^{NiO/Ga_2O_3}_{Ni\ 2p_{3/2}})$$

$$\Delta E_C = (E_g^{Ga_2O_3} - E_g^{NiO}) - \Delta E_V$$

where ΔE_V = VBO and conduction band offset ΔE_C = CBO. $E_g^{Ga_2O_3}$ is the band gap of Ga_2O_3 (4.80 eV) and E_g^{NiO} is the band gap of NiO (3.60 eV), which can be seen from Figure 2b,c, respectively. $E^{NiO}_{Ni\ 2p_{3/2}}$ and $E^{Ga_2O_3}_{Ga\ 2p_{3/2}}$ are determined by the NiO films and Ga_2O_3 films, respectively. $E^{Ga_2O_3/NiO}_{Ga\ 2p_{3/2}}$ and $E^{Ga_2O_3/NiO}_{Ni2p_{3/2}}$ are determined by the NiO/Ga_2O_3 p−n junction. As shown in Figure 5, $E^{NiO}_{Ni\ 2p_{3/2}}$ and E^{NiO}_{VBM} of the NiO films are 854.98 and

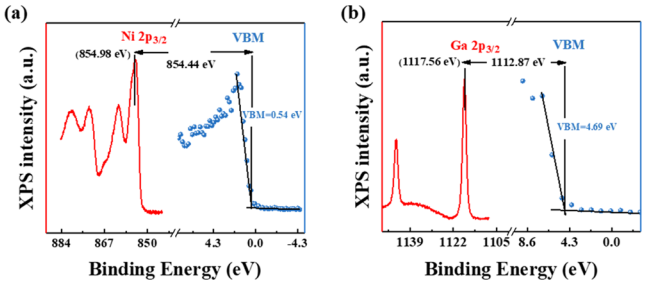

Figure 5. (a) Ni 2p and (b) Ga 2p core-level and valence band spectra for NiO and Ga_2O_3, respectively.

0.54 eV, respectively, and $E^{Ga_2O_3}_{Ga2p_{3/2}}$ and $E^{Ga_2O_3}_{VBM}$ of the Ga_2O_3 films are 1117.56 and 4.69 eV, respectively. Subsequently, by the following formulas

$$E^{NiO}_{Ni\ 2p_{3/2}-VBM} = (E^{NiO}_{Ni\ 2p_{3/2}} - E^{NiO}_{VBM})$$

$$E^{Ga_2O_3}_{Ga\ 2p_{3/2}-VBM} = (E^{Ga_2O_3}_{Ga\ 2p_{3/2}} - E^{Ga_2O_3}_{VBM})$$

The separation energies between the core level and the valence band maximum (VBM) can be calculated as follows: $E^{NiO}_{Ni2p_{3/2}-VBM}$ is 854.44 eV and $E^{Ga_2O_3}_{Ga2p_{3/2}-VBM}$ is 1112.87 eV.

Figure 6 reveals the Ga 2p and Ni 2p core-level spectrum of the NiO/Ga_2O_3 p−n junction. The value of $E^{NiO/Ga_2O_3}_{Ga2p_{3/2}}$ is 1117.08 eV and that of $E^{NiO/Ga_2O_3}_{Ni2p_{3/2}}$ is 855.63 eV. Therefore, the energy discrepancy between the Ga $2p_{3/2}$ and Ni $2p_{3/2}$ core

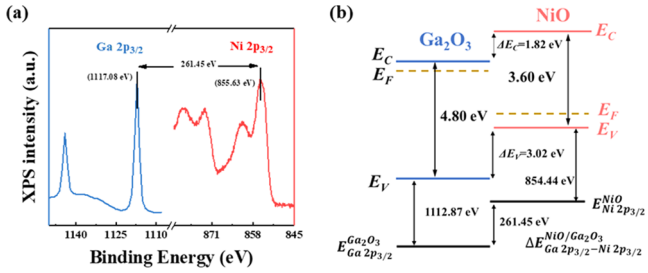

Figure 6. (a) Ga 2p and Ni 2p core levels for the NiO/Ga_2O_3 p−n junction. (b) Schematic representation of the band alignment at the NiO/Ga_2O_3 p−n junction interface.

levels is 261.45 eV, which can be calculated by the following formula

$$\Delta E^{NiO/Ga_2O_3}_{Ga\ 2p_{3/2}-Ni\ 2p_{3/2}} = (E^{NiO/Ga_2O_3}_{Ga\ 2p_{3/2}} - E^{NiO/Ga_2O_3}_{Ni\ 2p_{3/2}})$$

According to the above results, we can calculate the VBO value to be ΔE_V = 3.02 eV.

Based on the values of $E_g^{Ga_2O_3}$ = 4.80 eV and E_g^{NiO} = 3.60 eV, the value of ΔE_C for the NiO/Ga_2O_3 p−n junction can be calculated to be 1.82 eV. As shown in Figure 6b, a type II band alignment occurs between the NiO/Ga_2O_3 p−n junction, which is consistent with the previous literature.[36,37,45]

With the widespread application of the UV photodetectors, the application environment of the device becomes more complex and changeable. In particular, for detecting a solar-blind UV light signal, photodetectors often need to work under the environment of an extremely low air density. Understanding the performance of the photodetectors under different atmospheres is of great significance to not only improve their stability and accuracy but also expand their application scenarios. Herein, the performances of a photodetector in the environments of air, oxygen, and vacuum have been measured. As shown in Figure 7a, the photocurrent of the NiO/Ga_2O_3 p−n junction photodetector increases as the test environment changes from low oxygen to high oxygen. Compared with the pure oxygen environment, the oxygen content in the atmosphere is less and so the photocurrent gain effect is not obvious. The maximum photocurrent value of 31.78 nA is observed under the oxygen environment. In the oxygen atmosphere, the surface defects like oxygen vacancies on the Ga_2O_3 films absorb numerous O_2 molecules to form O_2^- molecules [$O_2 + e^- \rightarrow O_2^-$]. When the films are exposed to light irradiation, the photogenerated holes migrate and recombine with O_2 molecules on the surface of the films. The unpaired electrons left behind in the films contribute to the photocurrent. Figure 7b,c shows the responsivity and detectivity of the photodetector. The maximum responsivity (147 μA/W) and detectivity (1.68×10^{10} jones) were obtained in the oxygen atmosphere. Figure 7d shows the photoresponse and their fitting curves. The rise and decay times of the photodetector are 0.69/3.95, 0.34/3.65, and 0.20/2.51 s, corresponding to the environments of oxygen, air, and vacuum, respectively. The slow photoresponse in the oxygen atmosphere is caused by the adsorption and desorption of charges by O_2. Table 1 lists the comparison of the main parameters of our all-oxide NiO/Ga_2O_3 p−n junction photodetector and other UV photodetectors. This is the first report of a self-powered UV photodetector, based on the NiO/Ga_2O_3 p−n junction, being prepared at room temperature and consisting of all-oxide semiconductors.[46,47] Compared with the crystalline photo-

https://dx.doi.org/10.1021/acsaelm.0c00301
ACS Appl. Electron. Mater. 2020, 2, 2032−2038

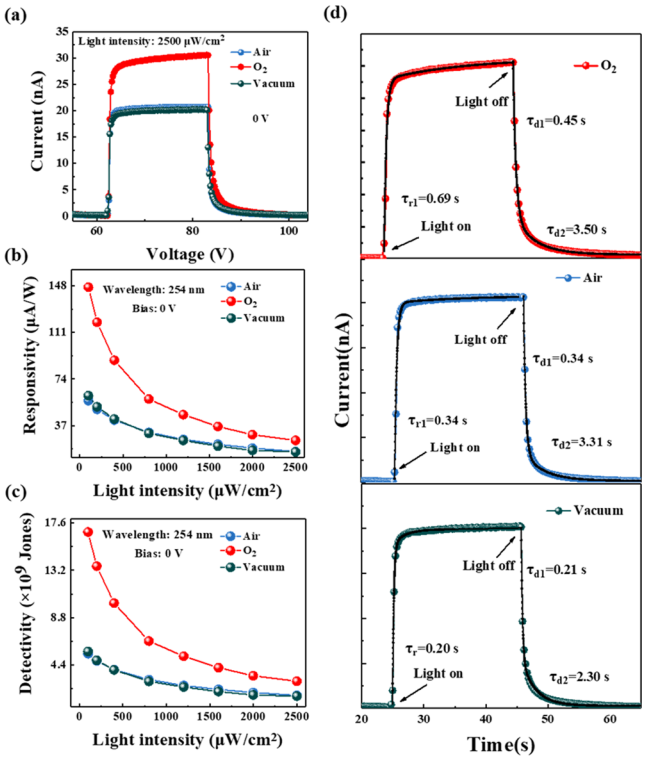

Figure 7. (a) Photoresponse of the photodetector in air, oxygen, and vacuum. (b) Responsivity as a function of the light intensity. (c) Detectivity as a function of the light intensity. (d) Enlarged view of the rise/decay edges and the corresponding exponential fitting.

detectors, which need to be prepared at high temperatures, all-oxide semiconductors photodetector in our work exhibit a lot of advantages such as easy preparation, low cost, and wide potential applications in flexible and wearable devices.[46,47] It is worth mentioning that the all-oxide NiO/Ga_2O_3 p−n junction is a potential structure for the self-powered photodetector, and the performance of the device will be greatly improved by optimizing the manufacturing parameters.

CONCLUSIONS

In summary, we fabricated a self-powered photodetector based on the all-oxide NiO/Ga_2O_3 p−n junction using a RF magnetron sputtering on the *c*-plane (0001) Al_2O_3 substrate at room temperature. The p−n junction exhibits an emblematic rectification characteristic. Thanks to the large built-in electric field, the photogenerated electron−hole pairs could be separated rapidly without any external power supply. The fabricated photodetector exhibits a fast response of 0.34/3.65 s (τ_r/τ_d), an I_{light}/I_{dark} ratio of 122, and a responsivity of 57 μA/W when exposed to a 254 nm irradiation at 0 V. Also, these results can broaden the development of self-powered UV photodetectors.

EXPERIMENTAL SECTION

Fabrication and Characteristics of the NiO/Ga_2O_3 p−n Junction. First, a 4 μm thick NiO film was deposited on the *c*-plane (0001) Al_2O_3 substrate by magnetron sputtering with a Ni target. The RF power was set at 300 W. An Ar/O_2 mixture gas with a 24/16 ratio and an atmospheric pressure of 2.0 Pa were the sputtering atmosphere. Second, the Ga_2O_3 thin films were deposited on the NiO films by RF magnetron sputtering from a Ga_2O_3 ceramic target. The RF power was set at 200 W. The working pressure and Ar gases flow rate were 1.0 Pa and 10 sccm, respectively. The chamber base pressure was 3.0×10^{-4} Pa, and all of the sputtered films were prepared at room temperature. X-ray diffraction (XRD) and field emission scanning electron microscopy (FE-SEM) were used to characterize the as-grown thin film morphology and crystallinity, respectively. A Hitachi U-3900 UV−vis spectrophotometer was used to analyze the ultraviolet−visible (UV−vis) absorption spectrum. X-ray photoelectron spectroscopy (XPS) was used to characterize the element content.

Preparation and Characterization of the Photodetector Based on the NiO/Ga_2O_3 p−n Junction. Graphene with an area of 0.5 cm^2 was transferred to the surface of Ga_2O_3 to act as a transparent conductive electrode. Then, a ∼2 mm diameter point Ag electrode was deposited on both graphene and NiO films to construct a photodetector. The devices' current−voltage (*I*−*V*) property and the time-dependent photoresponse feature were measured by Keithley 4200. All tests were carried out at room temperature.

AUTHOR INFORMATION

Corresponding Authors

Daoyou Guo − *Center for Optoelectronics Materials and Devices & Key Laboratory of Optical Field Manipulation of Zhejiang Province, Department of Physics, Zhejiang Sci-Tech University, Hangzhou 310018, China; State Key Laboratory of Silicon Materials, Zhejiang University, Hangzhou 310027, China;* orcid.org/0000-0002-6191-1655; Email: dyguo@zstu.edu.cn

Aiping Liu − *Center for Optoelectronics Materials and Devices & Key Laboratory of Optical Field Manipulation of Zhejiang Province, Department of Physics, Zhejiang Sci-Tech University,*

Table 1. Comparison of the Photoresponse Parameters of the NiO/Ga_2O_3 p−n Junction UV Photodetector with Those of the Other Previously Reported UV Photodetector Devices

photodetector	bias (V)	*R* (mA/W)	*D*	I_{photo}/I_{dark}	rise/decay time		ref
β-Ga_2O_3	1			13.3	0.62/8.97 s		5
β-Ga_2O_3	10			11.4	0.86/17.63 s		4
Au/Ga_2O_3	0	1×10^{-2}			1/100 μs		27
Ga_2O_3/NSTO	0	2.6		20	0.21/0.07 s		12
diamond/Ga_2O_3	0	0.2	6.9×10^9	37			48
graphene/*β*-Ga_2O_3/graphene	5	1.05×10^3		3.3×10^5	4.5/2.2 s		39
GaN/Ga_2O_3	0	2.84×10^1	6.17×10^{10}	74	0.14/0.07 s		20
Au/NiO/Au	5	4.5×10^3			0.27/0.20 s		34
NiO/*β*-Ga_2O_3	−7	4.15×10^2					38
NiO/Ga_2O_3	0	5.7×10^{-2}	5.45×10^9	122	0.34/3.65 s	air	this work
	0	6.1×10^{-2}	5.66×10^9	113	0.20/2.51 s	vacuum	
	0	1.47×10^{-1}	1.68×10^{10}	265	0.69/3.95 s	O_2	

https://dx.doi.org/10.1021/acsaelm.0c00301
ACS Appl. Electron. Mater. 2020, 2, 2032−2038

Hangzhou 310018, China; orcid.org/0000-0002-2338-062X; Email: liuaiping1979@gmail.com

Chaorong Li − *Center for Optoelectronics Materials and Devices & Key Laboratory of Optical Field Manipulation of Zhejiang Province, Department of Physics, Zhejiang Sci-Tech University, Hangzhou 310018, China*; Email: crli@zstu.edu.cn

Authors

Yachao Wang − *Center for Optoelectronics Materials and Devices & Key Laboratory of Optical Field Manipulation of Zhejiang Province, Department of Physics, Zhejiang Sci-Tech University, Hangzhou 310018, China*

Chao Wu − *Center for Optoelectronics Materials and Devices & Key Laboratory of Optical Field Manipulation of Zhejiang Province, Department of Physics, Zhejiang Sci-Tech University, Hangzhou 310018, China*

Peigang Li − *State Key Laboratory of Information Photonics and Optical Communications & Laboratory of Information Functional Materials and Devices, School of Science, Beijing University of Posts and Telecommunications, Beijing 100876, China*

Shunli Wang − *Center for Optoelectronics Materials and Devices & Key Laboratory of Optical Field Manipulation of Zhejiang Province, Department of Physics, Zhejiang Sci-Tech University, Hangzhou 310018, China*

Fengmin Wu − *Center for Optoelectronics Materials and Devices & Key Laboratory of Optical Field Manipulation of Zhejiang Province, Department of Physics, Zhejiang Sci-Tech University, Hangzhou 310018, China*

Weihua Tang − *State Key Laboratory of Information Photonics and Optical Communications & Laboratory of Information Functional Materials and Devices, School of Science, Beijing University of Posts and Telecommunications, Beijing 100876, China*

Complete contact information is available at: https://pubs.acs.org/10.1021/acsaelm.0c00301

Notes

The authors declare no competing financial interest.

■ ACKNOWLEDGMENTS

This work was supported by the National Natural Science Foundation of China (Nos. 61704153 and 61774019), the Zhejiang Public Service Technology Research Program/Analytical Test (LGC19F040001), the Natural Science Foundation of Zhejiang Province (No. LY20F040005), the Visiting Scholar Foundation of State Key Laboratory of Silicon Materials (SKL2019-08), and the Fundamental Research Funds of Zhejiang Sci-Tech University (2019Q061 and 2019Q067).

■ REFERENCES

(1) Razeghi, M. Short-wavelength solar-blind detectors-status, prospects, and markets. *Proc. IEEE* **2002**, *90*, 1006−1014.

(2) Chen, H.; Liu, K.; Hu, L.; Al-Ghamdi, A. A.; Fang, X. New concept ultraviolet photodetectors. *Mater. Today* **2015**, *18*, 493−502.

(3) Sang, L.; Liao, M.; Sumiya, M. A comprehensive review of semiconductor ultraviolet photodetectors: from thin film to one-dimensional nanostructures. *Sensors* **2013**, *13*, 10482−10518.

(4) Guo, D.; Wu, Z.; Li, P.; An, Y.; Liu, H.; Guo, X.; Yan, H.; Wang, G.; Sun, C.; Li, L.; Tang, W. Fabrication of β-Ga_2O_3 thin films and solar-blind photodetectors by laser MBE technology. *Opt. Mater. Express* **2014**, *4*, 1067−1076.

(5) Guo, D. Y.; Wu, Z. P.; An, Y. H.; Guo, X. C.; Chu, X. L.; Sun, C. L.; Li, L. H.; Li, P. G.; Tang, W. H. Oxygen vacancy tuned Ohmic-Schottky conversion for enhanced performance in β-Ga_2O_3 solar-blind ultraviolet photodetectors. *Appl. Phys. Lett.* **2014**, *105*, No. 023507.

(6) Luan, S.; Dong, L.; Ma, X.; Jia, R. The further investigation of N-doped β-Ga_2O_3 thin films with native defects for Schottky-barrier diode. *J. Alloys Compd.* **2020**, *812*, No. 152026.

(7) Wang, H.; Chen, H.; Li, L.; Wang, Y.; Su, L.; Bian, W.; Li, B.; Fang, X. High Responsivity and High Rejection Ratio of Self-Powered Solar-Blind Ultraviolet Photodetector Based on PEDOT:PSS/beta-Ga_2O_3 Organic/Inorganic p-n Junction. *J. Phys. Chem. Lett.* **2019**, *10*, 6850−6856.

(8) Wang, Y.; Li, L.; Wang, H.; Su, L.; Chen, H.; Bian, W.; Ma, J.; Li, B.; Liu, Z.; Shen, A. An ultrahigh responsivity self-powered solar-blind photodetector based on a centimeter-sized beta-Ga_2O_3/polyaniline heterojunction. *Nanoscale* **2020**, *12*, 1406−1413.

(9) Qin, Y.; Long, S.; Dong, H.; He, Q.; Jian, G.; Zhang, Y.; Hou, X.; Tan, P.; Zhang, Z.; Lv, H.; Liu, Q.; Liu, M. Review of deep ultraviolet photodetector based on gallium oxide. *Chin. Phys. B* **2019**, *28*, No. 018501.

(10) Chen, X.; Ren, F.; Gu, S.; Ye, J. Review of gallium-oxide-based solar-blind ultraviolet photodetectors. *Photonics Res.* **2019**, *7*, 381−415.

(11) Su, L.; Yang, W.; Cai, J.; Chen, H.; Fang, X. Self-Powered Ultraviolet Photodetectors Driven by Built-In Electric Field. *Small* **2017**, *13*, No. 1701687.

(12) Guo, D.; Liu, H.; Li, P.; Wu, Z.; Wang, S.; Cui, C.; Li, C.; Tang, W. Zero-Power-Consumption Solar-Blind Photodetector Based on beta-Ga_2O_3/NSTO Heterojunction. *ACS Appl. Mater. Interfaces* **2017**, *9*, 1619−1628.

(13) Wu, Z.; Jiao, L.; Wang, X.; Guo, D.; Li, W.; Li, L.; Huang, F.; Tang, W. A self-powered deep-ultraviolet photodetector based on an epitaxial Ga_2O_3/Ga:ZnO heterojunction. *J. Mater. Chem. C* **2017**, *5*, 8688−8693.

(14) Dong, L.; Yu, J.; Zhang, Y.; Jia, R. Elements (Si, Sn, and Mg) doped α-Ga_2O_3: First-principles investigations and predictions. *Comput. Mater. Sci. C* **2019**, *156*, 273−279.

(15) Wu, C.; Guo, D. Y.; Zhang, L. Y.; Li, P. G.; Zhang, F. B.; Tan, C. K.; Wang, S. L.; Liu, A. P.; Wu, F. M.; Tang, W. H. Systematic investigation of the growth kinetics of β-Ga_2O_3 epilayer by plasma enhanced chemical vapor deposition. *Appl. Phys. Lett.* **2020**, *116*, No. 072102.

(16) Guo, D.; Guo, Q.; Chen, Z.; Wu, Z.; Li, P.; Tang, W. Review of Ga_2O_3 based optoelectronic devices. *Mater. Today Phys.* **2019**, *11*, No. 100157.

(17) Guo, D. Y.; Li, P. G.; Chen, Z. W.; Wu, Z. P.; Tang, W. H.Ultra-wide bandgap semiconductor of β-Ga_2O_3 and its research progress of deep ultraviolet transparent electrode and solar-blind photodetector. *Acta Phys. Sin.68* (7), 078501.

(18) Zhang, J.; Shi, J.; Qi, D.-C.; Chen, L.; Zhang, K. H. Recent progress on the electronic structure, defect, and doping properties of Ga_2O_3. *APL Mater.* **2020**, *8*, No. 020906.

(19) Weng, W. Y.; Hsueh, T. J.; Chang, S. J.; Huang, G. J.; Hsueh, H. T. A β-Ga_2O_3/GaN Hetero-Structured Solar-Blind and Visible-Blind Dual-Band Photodetector. *IEEE Sens. J.* **2011**, *11*, 1491−1492.

(20) Li, P.; Shi, H.; Chen, K.; Guo, D.; Cui, W.; Zhi, Y.; Wang, S.; Wu, Z.; Chen, Z.; Tang, W. Construction of GaN/Ga_2O_3 p−n junction for an extremely high responsivity self-powered UV photodetector. *J. Mater. Chem. C* **2017**, *5*, 10562−10570.

(21) Guo, D.; Su, Y.; Shi, H.; Li, P.; Zhao, N.; Ye, J.; Wang, S.; Liu, A.; Chen, Z.; Li, C.; Tang, W. Self-Powered Ultraviolet Photodetector with Superhigh Photoresponsivity (3.05 A/W) Based on the GaN/Sn:Ga_2O_3 pn Junction. *ACS Nano* **2018**, *12*, 12827−12835.

(22) Nakagomi, S.; Momo, T.; Takahashi, S.; Kokubun, Y. Deep ultraviolet photodiodes based on β-Ga_2O_3/SiC heterojunction. *Appl. Phys. Lett.* **2013**, *103*, No. 072105.

(23) Qu, Y.; Wu, Z.; Ai, M.; Guo, D.; An, Y.; Yang, H.; Li, L.; Tang, W. Enhanced Ga_2O_3/SiC ultraviolet photodetector with graphene top electrodes. *J. Alloys Compd.* **2016**, *680*, 247−251.
(24) Yu, J.; Dong, L.; Peng, B.; Yuan, L.; Huang, Y.; Zhang, L.; Zhang, Y.; Jia, R. Self-powered photodetectors based on β-Ga_2O_3/4H−SiC heterojunction with ultrahigh current on/off ratio and fast response. *J. Alloys Compd.* **2020**, *821*, No. 153532.
(25) Yu, J.; Nie, Z.; Dong, L.; Yuan, L.; Li, D.; Huang, Y.; Zhang, L.; Zhang, Y.; Jia, R. Influence of annealing temperature on structure and photoelectrical performance of β-Ga_2O_3/4H-SiC heterojunction photodetectors. *J. Alloys Compd.* **2019**, *798*, 458−466.
(26) Guo, D. Y.; Chen, K.; Wang, S. L.; Wu, F. M.; Liu, A. P.; Li, C. R.; Li, P. G.; Tan, C. K.; Tang, W. H. Self-Powered Solar-Blind Photodetectors Based on α/β Phase Junction of Ga_2O_3. *Phys. Rev. Appl.* **2020**, *13*, No. 024051.
(27) Chen, X.; Liu, K.; Zhang, Z.; Wang, C.; Li, B.; Zhao, H.; Zhao, D.; Shen, D. Self-Powered Solar-Blind Photodetector with Fast Response Based on Au/beta-Ga_2O_3 Nanowires Array Film Schottky Junction. *ACS Appl. Mater. Interfaces* **2016**, *8*, 4185−4191.
(28) Shen, Y.; Yan, X.; Bai, Z.; Zheng, X.; Sun, Y.; Liu, Y.; Lin, P.; Chen, X.; Zhang, Y. A self-powered ultraviolet photodetector based on solution-processed p-NiO/n-ZnO nanorod array heterojunction. *RSC Adv.* **2015**, *5*, 5976−5981.
(29) Hakim, A.; Hossain, J.; Khan, K. A. Temperature effect on the electrical properties of undoped NiO thin films. *Renewable Energy* **2009**, *34*, 2625−2629.
(30) Xia, X. H.; Tu, J. P.; Zhang, J.; Wang, X. L.; Zhang, W. K.; Huang, H. Electrochromic properties of porous NiO thin films prepared by a chemical bath deposition. *Sol. Energy Mater. Sol. Cells* **2008**, *92*, 628−633.
(31) Patil, P.; Kadam, L. Preparation and characterization of spray pyrolyzed nickel oxide (NiO) thin films. *Appl. Surf. Sci.* **2002**, *199*, 211−221.
(32) Ahmed, A. A.; Afzal, N.; Devarajan, M.; Subramani, S. Structural, morphological, optical and electrical properties of NiO films prepared on Si (100) and glass substrates at different thicknesses. *Mater. Res. Express* **2016**, *3*, No. 116405.
(33) Wei, C.; Xu, J.; Shi, S.; Cao, R.; Chen, J.; Dong, H.; Zhang, X.; Yin, S.; Li, L. Self-powered visible-blind UV photodetectors based on p-NiO nanoflakes/n-ZnO nanorod arrays with an MgO interfacial layer. *J. Mater. Chem. C* **2019**, *7*, 9369−9379.
(34) Ahmed, A. A.; Devarajan, M.; Afzal, N. Fabrication and characterization of high performance MSM UV photodetector based on NiO film. *Sens. Actuators, A* **2017**, *262*, 78−86.
(35) Nakagomi, S.; Kubo, S.; Kokubun, Y. The orientational relationship between monoclinic β-Ga_2O_3 and cubic NiO. *J. Cryst. Growth* **2016**, *445*, 73−77.
(36) Ghosh, S.; Baral, M.; Kamparath, R.; Singh, S. D.; Ganguli, T. Investigations on band commutativity at all oxide p-type NiO/n-type β-Ga_2O_3 heterojunction using photoelectron spectroscopy. *Appl. Phys. Lett.* **2019**, *115*, No. 251603.
(37) Zhang, J.; Han, S.; Cui, M.; Xu, X.; Li, W.; Xu, H.; Jin, C.; Gu, M.; Chen, L.; Zhang, K. H. L. Fabrication and interfacial electronic structure of wide bandgap NiO and Ga_2O_3 pn heterojunction. *ACS Appl. Electron. Mater.* **2020**, *2*, 456−463.
(38) Li, K. H.; Alfaraj, N.; Kang, C. H.; Braic, L.; Hedhili, M. N.; Guo, Z.; Ng, T. K.; Ooi, B. S. Deep-Ultraviolet Photodetection Using Single-Crystalline beta-Ga_2O_3/NiO Heterojunctions. *ACS Appl. Mater. Interfaces* **2019**, *11*, 35095−35104.
(39) Li, Y.; Zhang, D.; Lin, R.; Zhang, Z.; Zheng, W.; Huang, F. Graphene Interdigital Electrodes for Improving Sensitivity in a Ga_2O_3:Zn Deep-Ultraviolet Photoconductive Detector. *ACS Appl. Mater. Interfaces* **2019**, *11*, 1013−1020.
(40) Lin, R.; Zheng, W.; Zhang, D.; Zhang, Z.; Liao, Q.; Yang, L.; Huang, F. High-Performance Graphene/beta-Ga_2O_3 Heterojunction Deep-Ultraviolet Photodetector with Hot-Electron Excited Carrier Multiplication. *ACS Appl. Mater. Interfaces* **2018**, *10*, 22419−22426.
(41) Ai, M.; Guo, D.; Qu, Y.; Cui, W.; Wu, Z.; Li, P.; Li, L.; Tang, W. Fast-response solar-blind ultraviolet photodetector with a graphene/β-Ga_2O_3/graphene hybrid structure. *J. Alloys Compd.* **2017**, *692*, 634−638.
(42) Qian, L.-X.; Wu, Z.-H.; Zhang, Y.-Y.; Lai, P. T.; Liu, X.-Z.; Li, Y.-R. Ultrahigh-Responsivity, Rapid-Recovery, Solar-Blind Photodetector Based on Highly Nonstoichiometric Amorphous Gallium Oxide. *ACS Photonics* **2017**, *4*, 2203−2211.
(43) Shayeganfar, F.; Vasu, K. S.; Nair, R. R.; Peeters, F. M.; Neek-Amal, M. Monolayer alkali and transition-metal monoxides: MgO, CaO, MnO, and NiO. *Phys. Rev. B* **2017**, *95*, No. 144109.
(44) Kraut, E. A.; Grant, R. W.; Waldrop, J. R.; Kowalczyk, S. P. Precise Determination of the Valence-Band Edge in X-Ray Photoemission Spectra: Application to Measurement of Semiconductor Interface Potentials. *Phys. Rev. Lett.* **1980**, *44*, 1620−1623.
(45) Kokubun, Y.; Kubo, S.; Nakagomi, S. All-oxide p−n heterojunction diodes comprising p-type NiO and n-type β-Ga_2O_3. *Appl. Phys. Express* **2016**, *9*, No. 091101.
(46) Lin, S.; Bai, X.; Wang, H.; Wang, H.; Song, J.; Huang, K.; Wang, C.; Wang, N.; Li, B.; Lei, M.; Wu, H. Roll-to-Roll Production of Transparent Silver-Nanofiber-Network Electrodes for Flexible Electrochromic Smart Windows. *Adv. Mater.* **2017**, *29*, No. 1703238.
(47) Lin, S.; Liu, J.; Li, W.; Wang, D.; Huang, Y.; Jia, C.; Li, Z.; Murtaza, M.; Wang, H.; Song, J.; Liu, Z.; Huang, K.; Zu, D.; Lei, M.; Hong, B.; Wu, H. A Flexible, Robust, and Gel-Free Electroencephalogram Electrode for Noninvasive Brain-Computer Interfaces. *Nano Lett.* **2019**, *19*, 6853−6861.
(48) Chen, Y.-C.; Lu, Y.-J.; Lin, C.-N.; Tian, Y.-Z.; Gao, C.-J.; Dong, L.; Shan, C.-X. Self-powered diamond/β-Ga_2O_3 photodetectors for solar-blind imaging. *J. Mater. Chem. C* **2018**, *6*, 5727−5732.

https://dx.doi.org/10.1021/acsaelm.0c00301
ACS Appl. Electron. Mater. 2020, 2, 2032−2038